Carbohydrate Polymers 157 (2017) 576–585

Contents lists available at ScienceDirect

Carbohydrate Polymers

journal homepage: www.elsevier.com/locate/carbpol

Effect of Cu(II) ions on the enhancement of tetracycline adsorption by Fe_3O_4@SiO_2-Chitosan/graphene oxide nanocomposite

Binyan Huang[a,b], Yunguo Liu[a,b,*], Bin Li[c], Shaobo Liu[d,e], Guangming Zeng[a,b], Zhiwei Zeng[a,b], Xiaohua Wang[a,b], Qimeng Ning[a,b], Bohong Zheng[e], Chunping Yang[a,b]

[a] College of Environmental Science and Engineering, Hunan University, Changsha 410082, PR China
[b] Key Laboratory of Environmental Biology and Pollution Control (Hunan University), Ministry of Education, Changsha 410082, PR China
[c] Changsha Economic and Technical Development Zone Water Purification Engineering Co.Ltd, Changsha 410100, PR China
[d] School of Metallurgy and Environment Central South University, Changsha 410083, PR China
[e] School of Architecture and Art Central South University, Changsha 410083, PR China

ARTICLE INFO

Article history:
Received 8 September 2016
Received in revised form 4 October 2016
Accepted 9 October 2016
Available online 12 October 2016

Keywords:
Graphene oxide
Chitosan
Tetracycline (TC)
Cu(II)
Adsorption

ABSTRACT

Fe_3O_4@SiO_2-Chitosan/GO (MSCG) nanocomposite was investigated by various techniques (SEM, TEM, XRD, VSM, FT-IR, XPS) for the removal of tetracycline (TC). Effects of pH, zeta potential and initial contaminant concentration were studied in detail. Four background cations (Na^+, K^+, Ca^{2+} and Mg^{2+}) with a concentration of 0.01 M showed little influence on the TC adsorption at the studied pH range while the divalent heavy metal cation Cu(II) could significantly enhance the adsorption. The results indicated that the highest adsorption capacity of TC were 183.47 mmol/kg and 67.57 mmol/kg on MSCG with and without Cu(II), respectively. According to mechanism investigation for the adsorption of TC by pH impact study and XPS analysis, besides electrostatic interaction and π–π interactions, the Cu(II) also acts as a bridge between TC and MSCG, which significantly improve the adsorption of TC. This study provided valuable guidance and effective method for the removal of TC from aquatic environments.

1. Introduction

Tetracycline (TC), the second most widely used antibiotics worldwide, has been extensively used as human medicines, veterinary drugs, and growth promoters in animal cultivation with little attention for a long time (Lian, Song, Liu, Zhu, & Xing, 2013). It is reported that only small amount of TC are absorbed during metabolism, and the majority are excreted via urine and feces as unchanged form. Residues of TC have been frequently detected in wastewater (Liu, Xu, Lee, Yu, & Lihong, 2016), surface water, and even in groundwater (Gottschall et al., 2012). Their presence within the environment may cause a risk to human health by promoting antibiotic resistant bacteria (ARB) and antibiotic resistance genes (ARG) (Sharma, Johnson, Cizmas, McDonald, & Kim, 2016). Therefore, to prevent its deleterious impact on the ecosystem and public health, it is of great importance to develop effective and low-cost technologies for its removal from surface and wastewater. To date, four most promising treatment methods are ion-exchange, membrane filtration, photocatalytic degradation, and adsorption. Compared to other techniques, adsorption is considered simple and economical, and remains one of the most attractive methods for antibiotic removal (Álvarez-Torrellas, Rodríguez, Ovejero, & García, 2016).

In environmental engineering, polymers have been used for different purposes, but the use of natural polymers has attracted considerable attention from the perspectives of cost, environmental and safety concern. Among these, chitosan is a highly deacetylated derivative of chitin, and known to be a biodegradable and non-toxic natural polymer in addition to its excellent capability of adsorption (Ge, Hua, & Chen, 2016). Previous studies have reported that chitosan and its derivatives as biosorbents have already been used in TC treatment (Jia et al., 2016). For example, Caroni et al. did a kinetic analysis of the sorption of TC on chitosan and reported that it is a promising sorbent for TC (Caroni, De Lima, Pereira, & Fonseca, 2009). Oladoja et al. explored a novel magnetic macro-reticulated cross-linked chitosan for the adsorption of TC from aquatic systems and high removal efficiencies were achieved (Oladoja, Adelagun, Ahmad, Unuabonah, & Bello, 2014). However, despite the numerous advantages and unique properties of chitosan, its use in a wider range of applications is limited because of its poor mechanical and electrical properties (Giannakas, Grigoriadi,

* Corresponding author at: College of Environmental Science and Engineering, Hunan University, Changsha 410082, PR China.
E-mail address: liuyunguohnu@163.com (Y. Liu).

http://dx.doi.org/10.1016/j.carbpol.2016.10.025
0144-8617/

Leontiou, Barkoula, & Ladavos, 2014). An effective method for improving the physical and mechanical properties of CS is to form organic–inorganic composites through incorporation of nanofillers, such as metal nanoparticles, clays, carbon nanotubes and graphene oxide (Huang et al., 2015).

Graphene, a monolayer of hexagonally arrayed sp^2-bonded carbon atoms, due to its excellent physical and chemical properties, has been studied world-wide for several purposes, since its discovery in 2004 (Kyzas, Koltsakidou, Nanaki, Bikiaris, & Lambropoulou, 2015). Chemical structure of graphene oxide (GO) is reported as oxidized graphene, decorated with various oxygenated functionalities such as hydroxy, epoxy on the basal plane and carbonyl, carboxylic acid at the edges (Mukherjee, Bhunia, & De, 2016).These oxygen hydrophilic functionalities make GO dispersible in water as well as some organic solvents extensively, and easier to intercalate. From earlier reported literatures, it is known that the aromatic compound can be easily adsorbed on GO and graphene by π− π stacking (Lin, Xu, & Li, 2013). TC consists of four aromatic rings with various functional groups on each ring, which can be strongly deposited on the GO surface via π–π interaction and cation–π bonding. Therefore, intercalation of CS into GO could not only enhance the physical and chemical properties derived synergistically from both components but also the adsorption capacity of TC.

Since this composite material is preferably soluble in water, separation is difficult. To improve the efficiency of separation, magnetic separation technology has attracted much attention (Han, Cao, Ouyang, Sohi, & Chen, 2016; Tang et al., 2012), but fewer were used to separate TC from aqueous solution directly. Thus, introducing magnetic properties to the adsorbent can be a research hotspot, magnetic nanoparticles, especially Fe_3O_4, have attracted more and more attentions because of the outstanding properties such as easy separation and low toxicity (Shan, Yan, Yang, Hao, & Du, 2015). However, there are two major challenges. One is related to the reunion, poor dispersion of Fe_3O_4 in water. The other is the easy oxidation/dissolution of iron nanoparticles, especially at high concentrations of acid solution. To compensate for these shortages, surface modifications of magnetic nanoparticles based on covalent binding or physical coating have been widely explored (Fan, Li, Zhou, & Liu, 2016; Muliwa, Leswifi, Onyango, & Maity, 2016). For example, Magnetic Fe_3O_4@poly(m-phenylenediamine) particles (Fe_3O_4@ PmPDs) with well-defined core−shell structure were designed for high performance Cr(VI) removal by taking advantages of the easy separation property of magnetic nanoparticles (Wang et al., 2015). In comparison with these organic coating materials, SiO_2 can serve as a more ideal shell component because of its stability under acidic conditions, and abundance of surface hydroxyl groups are able to link special functional groups (Lai, Xie, Chi, Gu, & Wu, 2016). Thus, the silica shell is convenient for the material to be grafted onto chitosan, which can also make the core–shell structure more stable.

The objective of this paper focused on the TC removal ability by the graphene oxide composites, namely Fe_3O_4@SiO_2-Chitosan/GO nanocomposite (MSCG). The samples were characterized by X-ray diffraction (XRD), scanning electron microscopy (SEM), transmission electron microscopy (TEM), Fourier transformation infrared spectrum (FT-IR), vibrating sample magnetometer (VSM) and X-ray photoelectron spectroscopy (XPS). Meanwhile, to fully understand the sorption behavior of TC on MSCG, and how pH and Cu(II) affect TC adsorption on the MSCG, a series of sorption experiments were conducted to determine the sorption properties. The adsorption mechanism was investigated by XPS analysis. Our results demonstrate that MSCG exhibits tremendous potential for effective removal of TC and fast separation performance in aqueous media simultaneously.

2. Materials and methods

2.1. Materials

Tetracycline hydrochloride (TC, 98% purity) was obtained from Amresco (Ohio, USA), and used without further purification. Chitosan (95% degree of deacetylation) was commercially available from Macklin Biochemical Co., Ltd. (Shanghai, China). Poly (4-styrenesulfonic acid-co-maleic acid) sodium salt (molar ratio 1:1) (PSSMA) was supplied by Aladdin (Shanghai, China). Analytical reagent grade copper chloride dihydrate ($CuCl_2{\cdot}2H_2O$), $FeCl_3{\cdot}6H_2O$, ethylsilicate (TEOS), anhydrous sodium acetate (CH_3COONa), glutaraldehyde solution (50 wt.%) and all other chemicals used in this study were purchased from Sinopharm Chemical Reagent Co., Ltd. (Shanghai, China). Milli-Q element ultrapure water (18.2 Ω, Millipore, Massachusetts) was used to prepare all solutions and all materials were used as-received without further treatment.

2.2. Preparation of Fe_3O_4@SiO_2

0.5 g PSSMA was dissolved in 20 mL of ethylene glycol to form a clear solution, and 0.54 g of $FeCl_3{\cdot}6H_2O$ and 1.5 g of anhydrous sodium acetate were added immediately under stirring until they were completely dissolved. Then the mixture was transferred into a Teflon lined stainless steel autoclave, and maintained at 473 K for 10 h, and then allowed to cool to room temperature. Finally the resulting products (Fe_3O_4 particles) were collected by magnetic separation, washed several times by distilled water and dried in the vacuum oven at 303 K. After that the Fe_3O_4 particles were dispersed in 6 mL of water and reserved.

The 1 mL as-prepared Fe_3O_4 dispersion was added into the mixed solution of 20 mL ethanol, 1 mL water and 1 mL NH_3 H_2O with the help of ultrasonication. Subsequently 0.1 mL TEOS and 5 mL ethanol were added into the reaction system simultaneously, and continued to ultrasonic. The obtained product (Fe_3O_4@SiO_2) was collected by magnetic separation and rinsed with ethanol several times.

2.3. Preparation of Fe_3O_4@SiO_2-Chitosan/GO(MSCG)

Graphene oxide (GO) was prepared following the methods described in our previous paper (Huang et al., 2015). The preparation process of MSCG following the method reported in the literature (Travlou, Kyzas, Lazaridis, & Deliyanni, 2013). Briefly, 2 g pure chitosan was dissolved in 100 mL of acetic solution (2% v/v), and the mixture was sonicated for 30 min. Then 0.75 g magnetic particles (Fe_3O_4@SiO_2) was added to the chitosan solution, and the mixture solution was stirred for 2 h. Next, 15 mL of glutaraldehyde solution was added to the reaction flask, together with 1.5 g of GO. The mixture was adjusted to pH 9.0–10.0 and was stirred at 353 K for 1 h. The precipitate was washed with ethanol and distilled water in turn and dried in a vacuum oven at 323 K. The final product (MSCG) was ground to a fine powder, with a size after sieving in the range of 75–125 μm.

2.4. Characterization

The morphological investigations of MSCG were observed by the field emission scanning electron microscope (SEM, Hitachi S-4800, Japan) and transmission electron microscopy (TEM, Tencnai G2 F20, USA). Fourier transform infrared spectrum (FT-IR, Nicolet Magna-IR 750, USA) was utilized for the identification of the surface functional groups at room temperature. Surface elemental composition of all samples were determined using a X-ray photoelectron spectroscopy (XPS) (Thermo Fisher Scientic, UK). Wide angle X-ray diffraction (XRD) patterns were recorded by a D8 ADVANCE X-ray

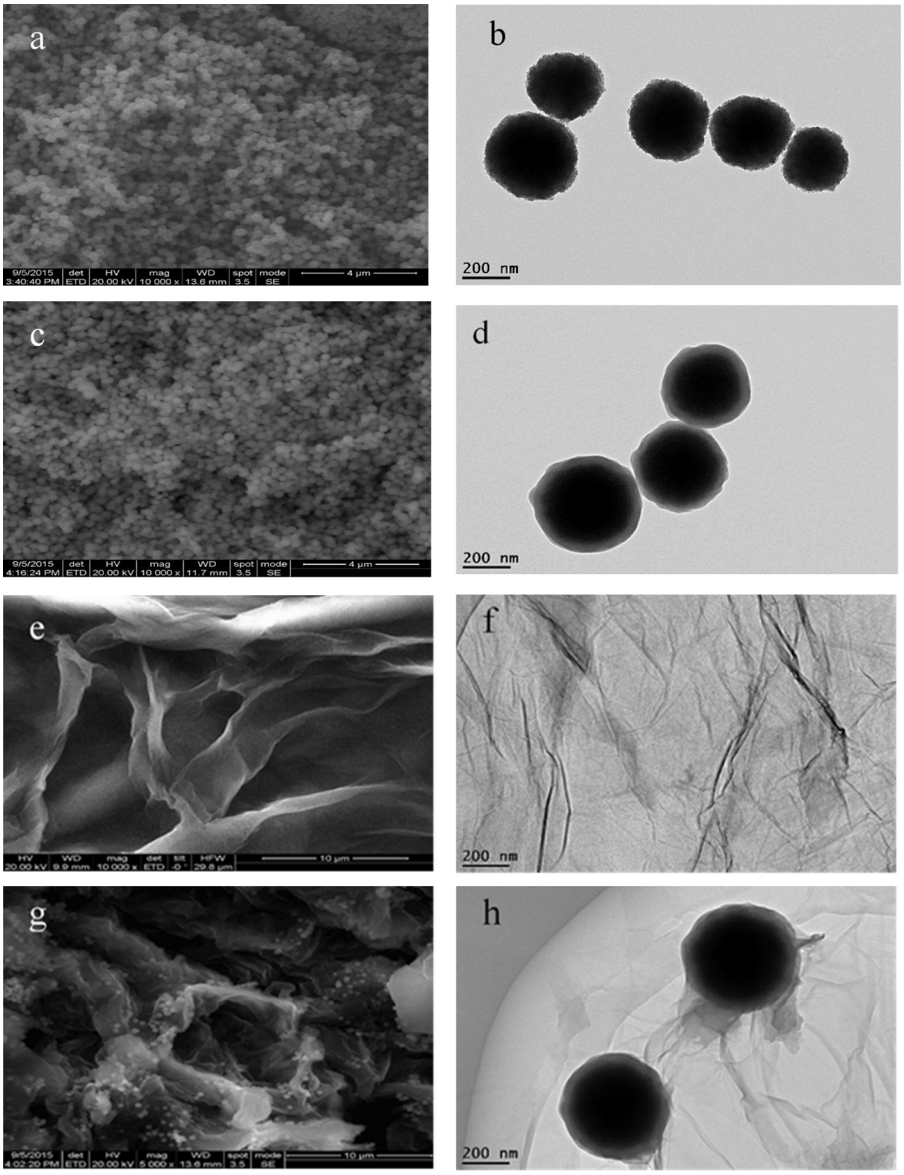

Fig. 1. The SEM images of (a) Fe_3O_4, (c) Fe_3O_4@SiO_2, (e) GO, (g) MSCG; The TEM images of (b). Fe_3O_4, (d) Fe_3O_4@SiO_2, (f) GO, (h) MSCG.

diffraction spectrometer (Bruker, German). Magnetic property of the sorbents was analyzed using a vibrating sample magnetometer (VSM, MPMS-XL-7). The point of zero surface charge (pH_{PZC}) of the samples was determined using a Zeta-sizer Nano-ZS (Malvern, UK).

2.5. Adsorption experiments

All experiments were conducted in100 mL glass bottles at 298 K, and all solutions were wrapped with aluminum foil to avoid light exposure. After 24 h of reaction, the mixture was drawn and separated immediately by the aid of a permanent magnet. TC concentrations before and after adsorption were determined by a UV spectrophotometer (UV-2550, SHIMADZU, Japan) at 358 nm. In this study, all experiments were duplicated, and only the average values were reported. Preliminary experiments (adsorbent free) showed that the loss of TC was less than 5% during the whole experimental process, (data not shown). The Cu(II) concentrations were determined by a flame atomic absorption spectrometry (PerkinElmer AA700, USA).

2.5.1. pH effect study

The effect of pH on TC adsorption on MSCG in the presence of four background electrolytes were conducted as follows. First, five sets of 50 mL solutions were prepared. Four sets of the solutions contained TC concentration of 0.1 mmol/L and 0.01 mol/L NaCl, KCl, $CaCl_2$, and $MgCl_2$ solution, respectively. Another set contained TC concentration of 0.1 mmol/L. 0.1 mol/L HCl or 0.1 mol/L NaOH was used to adjust the solution pH to the desired values in the range of 3.0–10.0. Then 20 mg MSCG was added into the solutions, and the mixtures were shaken with a speed of 150 rpm for 24 h. Finally, the concentrations of TC was analyzed.

The effect of pH on TC adsorption on MSCG with or without Cu(II) was conducted in a similar way as noted above. Three sets of 50 mL solutions were prepared. Two sets of the solutions contained TC concentration of 0.1 mmol/L and Cu(II) concentration of 0.1 or 0.2 mmol/L. Another set contained TC concentration of 0.1 mmol/L. 0.1 mol/L HCl or 0.1 mol/L NaOH was used to adjust the solution pH to the desired values in the range of 3.0–10.0. Then 20 mg MSCG was added into the solutions, and the mixtures were shaken with a speed of 150 rpm for 24 h. Finally, the concentrations of TC was analyzed.

2.5.2. Adsorption kinetics study

In the kinetic experiments, three sets of 1L solutions with TC concentration of 0.1 mmol/L, simultaneous TC concentration of 0.1 mmol/L and Cu(II) concentration of 0.1 mmol/L, and simultaneous TC concentration of 0.1 mmol/L and Cu(II) concentration of 0.2 mmol/L, were prepared respectively. The adsorbent was then added into the solution with a dosage of 0.4 g/L. The mixed solution was shaken with a speed of 150 rpm in darkness. HCl and NaOH solutions with the concentration of 0.1 M were used to adjust the pH to 6.0 ± 0.1. The samples were collected at appropriate time intervals, and the TC concentrations of all samples were measured. The amounts of TC adsorbed at specific time were determined by Eq. (1)

$$q_t = \frac{(C_0 - C_t)V}{m} \quad (1)$$

where q_t (mmol/kg) is the amount of TC adsorbed at time t, and C_t (mmol/L) is the concentration of TC at time t, V is the volume of TC solution, and m is the weight of MSCG.

2.5.3. Adsorption isotherms study

Adsorption isotherms of TC with or without Cu(II) were studied as follows. A series of 50 mL solutions with TC concentrations of 0–0.2 mM, with or without 0.1 or 0.2 mM Cu(II) were prepared.

The adsorbent was then added into the solutions with a dosage of 0.4 g/L and the solution pH was kept at 6.0 ± 0.1. Other experimental conditions were the same as the pH effect experiments. The equilibrium adsorption amounts of TC were calculated by Eq. (2)

$$q_e = \frac{(C_0 - C_e)V}{m} \quad (2)$$

where q_e (mmol/kg) is the amount of TC adsorbed at equilibrium, C_0 and C_e (mmol/L) are the concentration of TC at initial and equilibrium, respectively.

2.5.4. Reusability test

The regeneration of adsorbent was carried out by desorbing TC with 0.05 mol/L NaOH solution, TC/Cu with 0.05 mol/L HCl and 0.05 mol/L NaOH solutions, respectively. After being separated by the aid of a permanent magnet and washed with ultrapure water, the sorbent dried at 328 K for the next adsorption cycle. The amount of residual TC on the adsorbent was analyzed. The adsorption–desorption cycles were repeated for 5 times.

3. Results and discussion

3.1. Characterization of MSCG

Fig. 1 shows the magnification images of Fe_3O_4, Fe_3O_4@SiO_2, GO, MSCG. As shown in Fig. 1a and Fig. 1c, which represents the SEM of Fe_3O_4, Fe_3O_4@SiO_2, respectively, those nanoparticles are of spherelike morphology in general, in order to better observe the morphology and structure of the Fe_3O_4 and Fe_3O_4@SiO_2 nanoparticles, TEM measurements have been provided in Fig. 1b and d. As can be seen from Fig. 1b, the diameter of those particles is ranging between 250 and 300 nm, and the roughness of the nanoparticles surface can be discerned clearly, after being coated with a silica layer, the typical core–shell structure of the Fe_3O_4@SiO_2 can be observed, the surface becomes smoothly and the diameter increases to about 400 nm (Fig. 1d). Fig. 1e and f show a typical SEM and TEM image of GO, which presents a sheetlike structure with multi-layer smooth surface and wrinkled edge. After combination with Fe_3O_4@SiO_2 and chitosan to form the MSCG composite (Fig. 1g and h), the MSCG had a much rougher surface, revealing that many small Fe_3O_4@SiO_2-Chitosan particles had been assembled on the surface of the GO layers with a high density, and the construction of the Fe_3O_4@SiO_2-Chitosan particle was less than 1 μm as estimated from the TEM image.

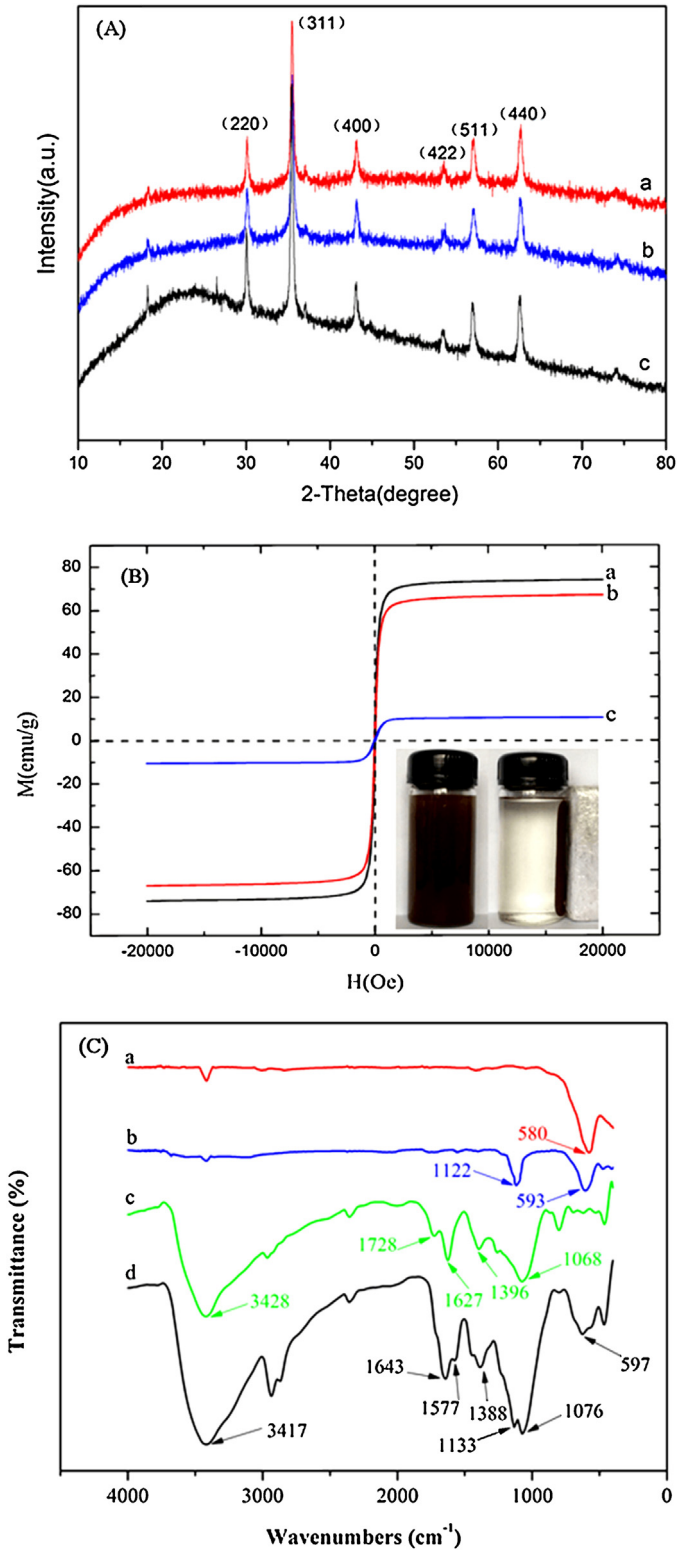

Fig. 2. (A) XRD patterns of (a) Fe_3O_4, (b) Fe_3O_4@SiO_2, (c) MSCG. (B) Magnetization curve of (a) Fe_3O_4, (b) Fe_3O_4@SiO_2, (c) MSCG. (The insets show the MSCG dispersed in ultrapure water and the magnetic separation). (C) FT-IR spectra of (a) Fe_3O_4, (b) Fe_3O_4@SiO_2, (c) GO, (d) MSCG.

Fig. 2A shows the XRD pattern of Fe_3O_4, Fe_3O_4@SiO_2 and MSCG. The strong diffraction peaks indexed to (220), (311), (400), (422),

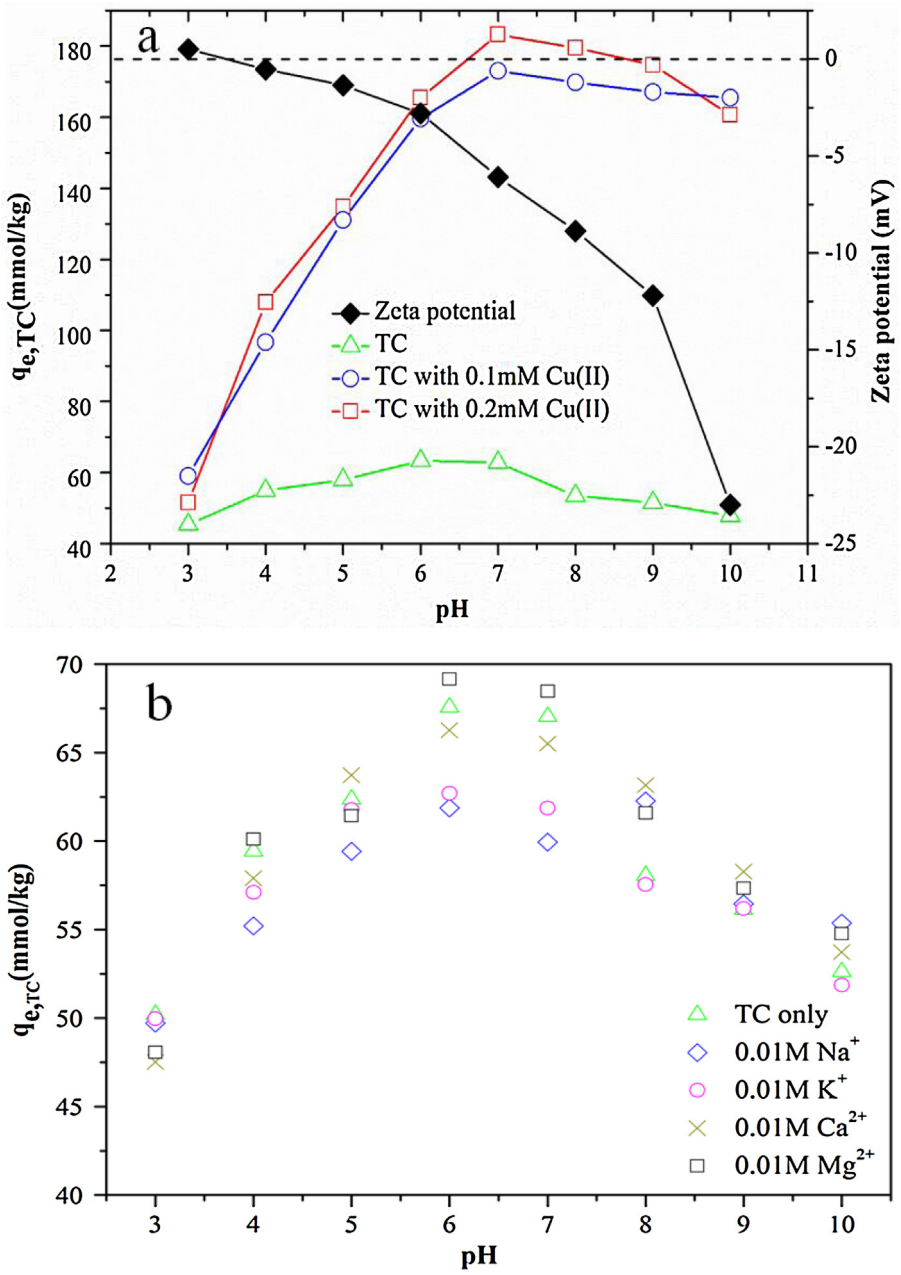

Fig. 3. (a) Zeta potentials of MSCG at different pH and effect of pH on adsorption of TC with and without Cu(II) by MSCG. (b) Adsorption of TC onto MSCG in four different metal cation electrolytes (Na^+, K^+, Ca^{2+}, and Mg^{2+}).

(511) and (440) show the characteristics of Fe_3O_4 with a cubic inverse spinel structure (JCPDS 19-0629) in all the samples. This result indicates that the multiple composite has been successfully synthesized without damaging the crystal structure of Fe_3O_4 core during silica coating and surface functionalization.

The room-temperature magnetization hysteresis loops were measured with a VSM to investigate the magnetic property of the sorbents. The saturation magnetization values for Fe_3O_4, Fe_3O_4@SiO_2 and MSCG were 74.0, 67.0 and 10.5 emu/g, respectively (Fig. 2B). Although the saturation magnetization decreased due to the relatively low amount of Fe_3O_4, the existence of GO and the surface modification by CS (Ye, Xie, Shi, Gao, & Ma, 2014), complete magnetic separation can be achieved in 30 s by placing a magnet near the vessels containing the aqueous dispersion of MSCG as shown in the inset of Fig. 2B. Additionally, no hysteresis was observed in the hysteresis loops of three materials, and the remanence and coercivity were nearly zero, exhibiting typical superparamagnetic behavior.

FT-IR was employed to examine the surface groups of the synthesized materials, and the FT-IR spectra of Fe_3O_4, Fe_3O_4@SiO_2, GO and MSCG were shown in Fig. 2C. The characteristic sorption band of Fe_3O_4 at 580 cm^{-1} was attributed to the stretching vibration of Fe–O bond (Singh, Barick, & Bahadur, 2011). Apart from the peak at 593 cm^{-1}, the spectra of Fe_3O_4@SiO_2 appeared a broad strong band at 1122 cm^{-1} due to Si—O stretching (Zhang et al., 2013), reflecting the coating of silica on the magnetite surface. As for the GO (Fig. 2C), absorption peak at 3428 cm^{-1} was attributed to O—H stretching vibration. The absorption at 1728 cm^{-1} corresponded to the stretching band of C=O in carboxylic acid (Hou, Zhang, Zhu, Li, & Wang, 2011). The peak at 1627 cm^{-1} could be assigned to the C=C stretching vibration of the sp^2 carbon skeletal network (Kyzas, Travlou, & Deliyanni, 2014). The peaks at 1396 cm^{-1} and

Table 1
Kinetic constants for the adsorption of TC with and without Cu(II) onto MSCG.

Initial concentration (mM)		Pseudo-first-order kinetic				Pseudo-second-order kinetic			
		$q_{e,exp}$ (mmol/kg)	k_1 (1/min)	$q_{e,cal}$ (mmol/kg)	R^2	$q_{e,exp}$ (mmol/kg)	k_2 (kg/mmol min)	$q_{e,cal}$ (mmol/kg)	R^2
TC = 0.1	Cu(II) = 0	57.80	2.50×10^{-3}	26.31	0.862	57.80	4.23×10^{-4}	59.38	0.997
	Cu(II) = 0.1	151.2	4.97×10^{-3}	18.89	0.694	151.2	13.4×10^{-4}	151.7	0.998
	Cu(II) = 0.2	151.4	3.53×10^{-3}	31.02	0.919	151.4	5.71×10^{-4}	152.2	0.998

1068 cm^{-1} corresponded to the stretching vibrations of C—OH and C—O—C, respectively (Wu et al., 2014). In comparison with the GO, the same functional groups above mentioned were found in the MSCG around the corresponding wavenumber. However, the peak at 1728 cm^{-1}, which can be attributed to carboxyl groups, disappeared for MSCG. The characteristic bands appeared at 1639 cm^{-1} ascribed to the amide I (C=O stretching), at 1596 cm^{-1} ascribed to amide II (N—H blending modes), confirming that the carboxyl groups reacted with chitosan during the preparation of the composite. In addition, the band at 3428 cm^{-1} and 1068 cm^{-1} presented a shift to 3417 cm^{-1} and 1076 cm^{-1}, respectively, and the characteristic peak of Fe_3O_4@SiO_2 could also be observed at 597 cm^{-1} and 1133 cm^{-1}, indicating Fe_3O_4@SiO_2 was successfully grafted to the surface of GO by the function of chitosan.

3.2. Effect of pH

As shown in Fig. S1a, the TC (symbolized as TCH_2) is an amphoteric molecule with multiple ionizable functional groups and formed a series of species at different pH levels. As can be seen from Fig. S1b, the predominate TC species are TCH_3^+ at pH <3.3, TCH_2^0 at 3.3 < pH <7.7, TCH^- at 7.7 < pH <9.7, and TC^{2-} at pH >9.7 (Gu & Karthikeyan, 2005). The TC becomes less positively charged (or more negatively charged) as pH is increased.

As shown in Fig. 3a, the pH_{PZC} of MSCG estimated by zeta potential was 3.0–4.0. When the pH was 3.0–4.0, zeta potential shift from positive to negative, indicating that the surface of MSCG was negatively charged over the pH range except pH 3.0. And it also shows that solution pH significantly affected TC adsorption on the MSCG. In the absence of Cu(II), the adsorption of TC increases when pH is increased from 3.0 to 6.0; then it gradually reduced as the pH is further increased (to pH 10.0). The pH effect can be associated with the pH of point of zero charge (pH_{PZC}) of MSCG and the pH-dependent speciation of TC. This result can be interpreted as follows. When the solution pH is below the pK_{a1} (3.3) value of TC, the dominant species of TC in water is TCH_3^+, while the surface of the adsorbent was positively charged. The dominant electrostatic interaction between TC and the MSCG should be repulsion at low pH. However, there is still a considerable amount of TC (50.21 mmol/kg) adsorbed on MSCG surfaces at pH 3.0, indicating that besides the electrostatic interaction, the strong π–π interactions could occur between the bulk π systems on GO surface and benzene rings in TC molecules (Lin et al., 2013). When solution pH increases from 3.3, the adsorption capacity increases with the highest adsorption capacity (67.57 mmol/kg) found at pH 6.0, which was much higher compared with the previous literatures in the adsorption of TC (Kang, Liu, Zheng, Qu, & Chen, 2010; Oladoja et al., 2014; Zhang, Liu, Wu, Lan, & Qu, 2015). At pH 6.0–7.0, the dominant TC species is TCH_2, and the MSCG surface is negatively charged. Hence, the lowest electrostatic repulsion is experienced at pH 6.0–7.0, resulting in the highest adsorption capacity. When pH further increases from 7.7, the dominant species become TCH^- and TC^{2-}, and the surface of MSCG was negatively charged. The increase in the proportion of negatively charged TC species and negative charges on the surfaces of MSCG results in a stronger electrostatic repulsion; thus, there is a reduced adsorption affinity of TC to MSCG, and the adsorption capacity reduced to 52.62 mmol/kg at pH 10.0.

The effects of four background cations (Na^+, K^+, Ca^{2+}, and Mg^{2+}) with a concentration of 0.01 M on the adsorption of TC onto MSCG over pH range from 3.0 to 10.0 were investigated by batch adsorption experiments, and the results were showed in Fig. 3b. For all four cation electrolytes, the adsorption of TC onto MSCG increased from 47.5 mmol/kg at pH 3.0 to 69.2 mmol/kg at pH 6.0, while without the four cation electrolytes, the adsorption of TC onto MSCG increased from 50.2 mmol/kg at pH 3.0 to 67.6 mmol/kg at pH 6.0. Thus, it obviously showed that the four background cations had little effect on the TC adsorption at the studied pH range, which was similar to the results reported in previous literature (Zhao, Geng, Wang, Gu & Gao, 2011).

Adsorption of TC onto MSCG with the presence of 0.1 mM and 0.2 mM Cu (II) in various pH values was shown in Fig. 3a. The results showed that the TC uptake increases tremendously in the presence of Cu(II) than the absence of Cu(II) as pH is increased from 3.0 to 7.0, and the adsorption amount of TC increases with the increasing concentration of Cu(II). For example, the highest adsorption capacity of TC with the presence of 0.1 mM and 0.2 mM Cu(II) were 173.60 mmol/kg and 183.47 mmol/kg at pH 7.0, respectively. This is mainly attributed to the effect that the TC species in the presence of Cu(II) carry more positive charges than TC species in the absence of Cu(II), which should increase the TC adsorption according to the rule of electrostatic interaction. This leads to a hypothesis that the Cu(II) act as a bridge between MSCG and TC. As the Cu(II) has higher affinity to the sorbent, the TC (complexed with Cu(II)) can be greatly adsorbed (Kang et al., 2010). While when the pH is increased from 7.0 to 10.0, the dominant species of TC are TCH^- and TC^{2-}, due to the increased electrostatic repulsion, the adsorption capacity of TC decreases in the presence of Cu(II). Similar observations were reported on the adsorption of TC on goethite and waste tire powder in the presence of Cu(II) (Lian et al., 2013; Zhao et al., 2011).

3.3. Adsorption kinetics

The adsorption kinetics of TC on GMSC with and without the presence of 0.1 mM and 0.2 mM Cu(II) was illustrated in Fig. 4a. For the single system, TC adsorption rapidly increased during the first 60 min, subsequently the adsorption rate declined, and the equilibrium was reached within 480 min. For the binary system, the presence of Cu(II) increased the adsorption rate of TC and enhanced the amount of absorbed TC to about treble values in the absence of Cu(II), and the equilibration time was significantly shorten to 240 min, however, the sorption of TC kept relatively constant with an increase in Cu(II) concentration in the range of 0.1–0.2 mM. Two commonly used kinetics models, pseudo-first-order and pseudo-second-order kinetics models were applied to interpret kinetics data. The linear forms of expressions are presented by Eqs. (3) and (4) below.

$$\ln(q_e - q_t) = \ln q_e - k_1 t \tag{3}$$

$$\frac{t}{q_t} = \frac{1}{k_2 q_e^2} + \frac{t}{q_e} \tag{4}$$

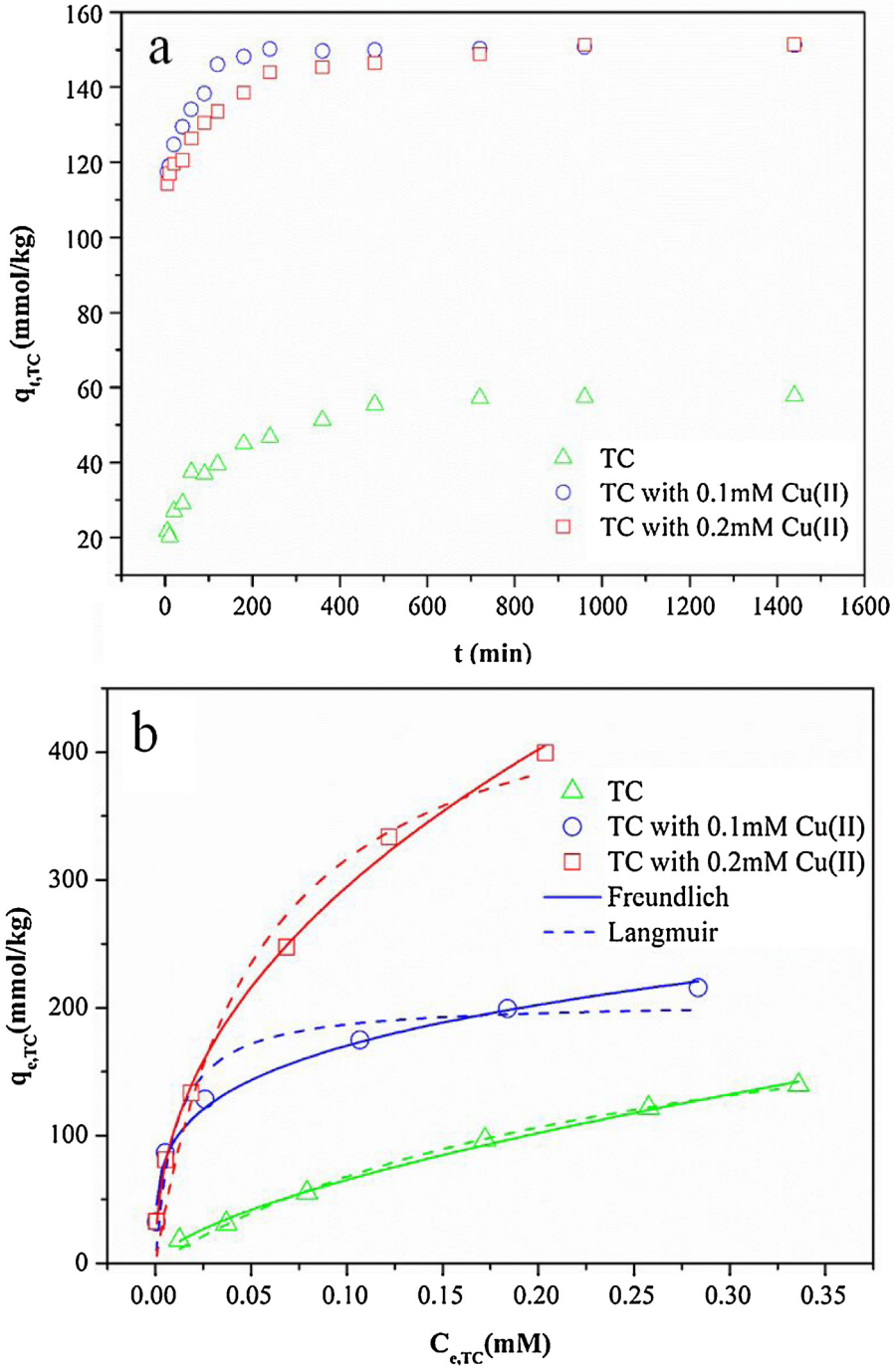

Fig. 4. (a) Adsorption kinetics of TC with and without Cu(II) onto MSCG. (b) Adsorption isotherms of TC with and without Cu(II) onto MSCG. (pH = 6 ± 0.1, T = 298 K, t = 24 h).

Table 2
Langmuir and Freundlich parameters for the adsorption of TC with and without Cu(II).

Initial concentration (mM)		Langmuir			Freundich		
		q_{max} (mmol/kg)	K_L (L/mmol)	R^2	K_F (mmol^{1-n} L^n/kg)	1/n	R^2
TC = 0.1	Cu(II) = 0	248.0	3.752	0.995	286.5	0.643	0.996
	Cu(II) = 0.1	205.3	101.7	0.917	302.0	0.249	0.987
	Cu(II) = 0.2	485.3	18.73	0.966	828.1	0.449	0.998

where q_e (mmol/kg) and q_t (mmol/kg) are the amount of TC adsorbed at equilibrium and at time t, k_1 (1/min) is the rate constant of pseudo-first order adsorption, while k_2(kg/mmol min) is the rate constant of pseudo-second order model.

The values of k_1, k_2, and q_e can be calculated from Eqs. (3) and (4), and are presented with the linear regression values in Table 1. As shown in Table 1, the adsorption kinetics data can be better fitted to the pseudo-second-order model ($R^2 > 0.99$), In addition, the

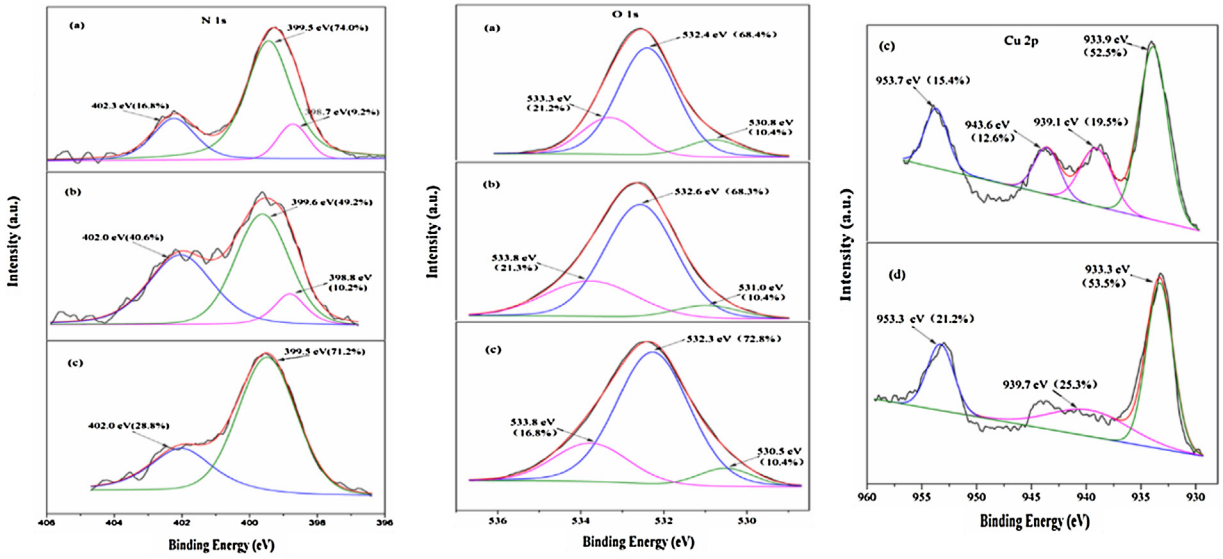

Fig. 5. The XPS spectra of N 1s, O 1s, Cu 2p on (a) MSCG; (b) TC-loaded MSCG; (c) TC/Cu(II)-loaded MSCG; (d) Cu(II)-loaded MSCG.

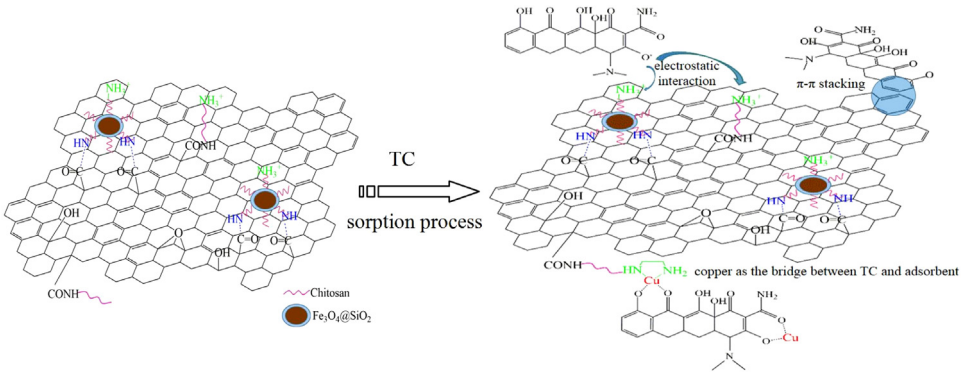

Fig. 6. Schematic adsorption mechanism for the removal of TC.

calculated q_e values were very close to the theoretical ones, which suggested that the dominant rate-limiting step of the adsorption mechanism might be due to chemical adsorption (Gao et al., 2012).

3.4. Adsorption isotherms

Adsorption isotherms of TC on MSCG at pH 6.0 with and without Cu(II) are shown in Fig. 4b. The amount of TC adsorbed on MSCG increased with increasing TC equilibrium concentration, and the adsorption amount of TC was significantly enhanced with the increasing concentration of Cu(II). The same phenomena was reported for the adsorption of TC onto mesoporous silica adsorbent (Zhang et al., 2015). Both Langmuir and Freundlich isotherm models are applied to analyze the adsorption process of TC with and without the presence of 0.1 mM and 0.2 mM Cu(II) to the composite MSCG, which are presented in Eqs. (5) and (6), respectively.

$$q_e = \frac{q_{\max} K_L C_e}{1 + K_L C_e} \quad (5)$$

$$q_e = K_F C_e^{1/n} \quad (6)$$

Where q_e (mmol/kg) is the TC adsorption amount at equilibrium, q_{max} (mmol/kg) is the capacity representing a full monolayer coverage of adsorbent surface according to Langmuir isotherm, C_e is the concentration of TC at equilibrium, K_L is the relative energy of adsorption, K_F is adsorption constant of Freundlich isotherm, and n is the Freundlich linearity index (Liu, Zhong, Zhao, Frear, & Zheng, 2015). The conformity of the experimental data to the two isotherm equations has been tested, as indicated by the values of the correlation coefficients (R^2) of the nonlinear plots, and the calculated parameters are listed in Table 2. Compared with the Langmuir model, the Freundlich model fits the adsorption isotherms better (R^2 = 0.996, 0.987, 0.997), which indicates that the uptake of TC with and without Cu(II) on the sorbent preferably followed the multilayer adsorption process. The values of K_F and $1/n$ for all the results suggested the adsorbent was favorable for the removal of TC from aqueous solution.

3.5. Removal mechanism

Considering that XPS is useful to identify the chemical elements on the surface of the adsorbent, to investigate the adsorption mechanism of TC and Cu(II) on MSCG, XPS analysis of MSCG before and after the adsorption of TC and TC/Cu have been carried out. The results of a wide scan of samples in Fig. S2 show that the major elements of MSCG and Cu-loaded MSCG are C, N, and O. The presence of a Cu(II) 2p peak in TC/Cu-loaded MSCG provides evidence of the Cu(II) adsorption onto the sorbent. The adsorption mechanism was studied as follows:

The high-resolution N 1s XPS spectra of the MSCG before and after adsorption are shown in Fig. 5. For MSCG, N 1s peak was deconvoluted into three peaks, 9.2% of —N = at 398.7 eV, 74.0% of —NH— at 399.5 eV and 16.8% of positively charged nitrogens (N^+)

at 402.3 eV, after TC adsorption, the molar ratio of N^+ increased significantly from 16.8% to 40.6%, the —N= increased from 9.2% to 10.2% and the —NH— decreased from 74.0% to 49.2%. The relative content of N^+ peak is much larger in the MSCG than in TC-loaded MSCG, which may be ascribed to the increase of N^+ peak as a result of the interaction between TC and amino groups in MSCG. The O1s spectra of MSCG were deconvoluted into three peaks at 530.4, 532.5 and 533.6 eV, which were assigned to the Fe—O (Fe_3O_4), C—O (alcohol hydroxyl and/or ether), and C=O (carbonyl), respectively (Travlou et al., 2013). Compared with the molar ratio change of the high-resolution N 1s XPS spectra, there is no obvious change for the high-resolution O1s XPS spectra before and after the adsorption of TC. Therefore, we can conclude that the positively charged nitrogens might be one of the most important adsorption driving forces for TC, indicating the presence of electrostatic interaction between TC and positively charged nitrogens in the MSCG according to the effect of pH. While another important adsorption force was the strong π–π interactions between the bulk π systems on GO surface and benzene rings in TC molecules based on the reports in the previous literatures (Gao et al., 2012; Lin et al., 2013). As shown in Fig. S3, the Cu(II) adsorption on MSCG with and without TC increases with the solution pH increases up to 7.0, then it changed little as the solution pH is further increased to 10.0. It also can be seen that the presence of TC greatly increases the adsorption amount of Cu(II) on the adsorbent. Generally, the saturation adsorption sites is certain for the adsorption of Cu(II) on the adsorbent, while the sorption amounts of Cu(II) on MSCG were increased significantly after the addition of TC. This is mainly due to a part of the copper was adsorbed on the surface of TC, which could be in the formation of TC-Cu(II) complexes (Tang et al., 2014; Zhang et al., 2015). In the Cu2p spectra (Fig. 5), the peaks should be assigned to the binding energy of the Cu(II) $2p_{3/2}$ and Cu(II) $2p_{1/2}$ level, respectively. A satellite band (939.1–943.6 eV) was observed nearby the Cu $2p_{3/2}$ peak (933 eV), which was representative of the oxidation state of Cu(II). It also can be seen from Fig. 5, when TC was added into the solution, the presence of TC leaded to the formation of a new satellite peak, suggesting that some of the oxygen-containing functional groups(C=O, —OH) on TC could combine with Cu(II), as the oxygen-containing functional groups exhibit strong affinity towards Cu(II). Meanwhile, the adsorption amount of TC was significantly enhanced with the increasing concentration of Cu(II), indicating the Cu(II) played a crucial important role in promoting the absorption of TC on MSCG. After TC uptake, only slight shifts of the three peaks of N 1s spectra were observed, when TC/Cu(II) were added, the peaks of —N= disappeared, and the molar ratio of —NH- increased significantly from 49.2% to 71.2%, which proved the adsorption interaction between Cu(II) and amino groups in MSCG. Due to the strong complexation between Cu(II) and amino groups of the adsorbent, the N atom donated a lone pair electrons to form the covalent bond N—Cu(II) (Ling, Liu, Xu, Chen, & Li, 2013). The same phenomena was reported for the adsorption of TC/Cu onto chelating amino-Fe(III) functionalized mesoporous silica (Zhang et al., 2015). After the adsorption of TC/Cu, the molar ratio of the C—O increased from 68.3% to 72.8% and the molar ratio of the C=O decreased from 21.3% to 16.8% compared with the adsorption of TC. This result can be attributed to the interaction of Cu(II) with oxygen in TC to form metal complexes, which may result in the content change of oxygen-containing functional groups of TC, and it's consistent with the XPS study of Cu(II). The XPS analysis of interaction between Cu(II) and MSCG, Cu(II) and TC as mentioned above demonstrated that the Cu(II) participated in a bridging interaction between TC and the adsorbent.

Based on the above results and discussion, the adsorption mechanism in this study was schematically described in Fig. 6. In single TC, the presence of electrostatic interaction between TC and positively charged nitrogens in the MSCG, and the strong π–π interactions between the bulk π systems on GO surface and benzene rings in TC molecules were the important adsorption force. After Cu(II) was involved, in the ternary system of MSCG, TC and Cu(II), the Cu(II) participated in a bridging interaction between TC and the adsorbent, including metal complexes by the interaction of Cu(II) with oxygen-containing functional groups of TC, and the strong complexation between Cu(II) and amino groups of the adsorbent. It's the role of Cu(II) that notably enhanced adsorption efficiency in the removal of the combined contaminants.

3.6. Reusability

The adsorption–desorption cycles were repeated five times, the results are shown in Fig. S4. Compared to the virgin composite MSCG, the regenerated MSCG exhibited excellent reusability for the adsorption of TC with and without Cu(II). At the 5th adsorption–desorption cycle, the adsorption capacity of TC with and without Cu(II) on the MSCG decreased to approximately 85.7% and 84.0% of the initial adsorption amounts, respectively, indicating that the MSCG could be an efficient and potential adsorbent for TC removal due to the excellent regeneration performance.

4. Conclusions

In this work, MSCG was successfully prepared which could be separated and collected easily from treated solution by an external magnetic field. Sorption results indicated that the experimental data were well-fitted to the pseudo-second-order kinetic model and Freundlich isotherm model. The underlying mechanism of TC adsorption was investigated by pH impact study and XPS analysis. The interaction between TC and MSCG might include electrostatic interaction and π–π interactions, the presence of Cu(II) in binary system significantly enhances the adsorption of TC on MSCG, indicating that the Cu(II) acts as a bridge between TC and MSCG.

Acknowledgements

This work was financially supported by the National Natural Science Foundation of China (Grant No. 41271332, 51521006 and 51478470), and the International S&T Cooperation Program of China (Project Contract No. 2015DFG92750).

Appendix A. Supplementary data

Supplementary data associated with this article can be found, in the online version, at http://dx.doi.org/10.1016/j.carbpol.2016.10.025.

References

Álvarez-Torrellas, S., Rodríguez, A., Ovejero, G., & García, J. (2016). Comparative adsorption performance of ibuprofen and tetracycline from aqueous solution by carbonaceous materials. *Chemical Engineering Journal*, *283*, 936–947.

Caroni, A., De Lima, C., Pereira, M., & Fonseca, J. (2009). The kinetics of adsorption of tetracycline on chitosan particles. *Journal of Colloid and Interface Science*, *340*(2), 182–191.

Fan, H.-L., Li, L., Zhou, S.-F., & Liu, Y.-Z. (2016). Continuous preparation of Fe_3O_4 nanoparticles combined with surface modification by L-cysteine and their application in heavy metal adsorption. *Ceramics International*, *42*(3), 4228–4237.

Gao, Y., Li, Y., Zhang, L., Huang, H., Hu, J., Shah, S. M., et al. (2012). Adsorption and removal of tetracycline antibiotics from aqueous solution by graphene oxide. *Journal of Colloid and Interface Science*, *368*(1), 540–546.

Ge, H., Hua, T., & Chen, X. (2016). Selective adsorption of lead on grafted and crosslinked chitosan nanoparticles prepared by using Pb^{2+} as template. *Journal of Hazardous Materials*, *308*, 225–232.

Giannakas, A., Grigoriadi, K., Leontiou, A., Barkoula, N. M., & Ladavos, A. (2014). Preparation, characterization: Mechanical and barrier properties investigation of chitosan-clay nanocomposites. *Carbohydrate Polymers*, *108*, 103–111.

Gottschall, N., Topp, E., Metcalfe, C., Edwards, M., Payne, M., Kleywegt, S., et al. (2012). Pharmaceutical and personal care products in groundwater, subsurface drainage, soil, and wheat grain, following a high single application of municipal biosolids to a field. *Chemosphere*, *87*(2), 194–203.

Gu, C., & Karthikeyan, K. (2005). Interaction of tetracycline with aluminum and iron hydrous oxides. *Environmental Science & Technology*, *39*(8), 2660–2667.

Han, Y., Cao, X., Ouyang, X., Sohi, S. P., & Chen, J. (2016). Adsorption kinetics of magnetic biochar derived from peanut hull on removal of Cr (VI) from aqueous solution: Effects of production conditions and particle size. *Chemosphere*, *145*, 336–341.

Hou, C., Zhang, Q., Zhu, M., Li, Y., & Wang, H. (2011). One-step synthesis of magnetically-functionalized reduced graphite sheets and their use in hydrogels. *Carbon*, *49*(1), 47–53.

Huang, B., Liu, Y., Li, B., Zeng, G., Hu, X., Zheng, B., et al. (2015). Synthesis of graphene oxide decorated with core@double-shell nanoparticles and application for Cr(VI) removal. *RSC Advances*, *5*(129), 106339–106349.

Jia, S., Yang, Z., Yang, W., Zhang, T., Zhang, S., Yang, X., et al. (2016). Removal of Cu (II) and tetracycline using an aromatic rings-functionalized chitosan-based flocculant: Enhanced interaction between the flocculant and the antibiotic. *Chemical Engineering Journal*, *283*, 495–503.

Kang, J., Liu, H., Zheng, Y. M., Qu, J., & Chen, J. P. (2010). Systematic study of synergistic and antagonistic effects on adsorption of tetracycline and copper onto a chitosan. *Journal of Colloid and Interface Science*, *344*(1), 117–125.

Kyzas, G. Z., Travlou, N. A., & Deliyanni, E. A. (2014). The role of chitosan as nanofiller of graphite oxide for the removal of toxic mercury ions. *Colloids and Surfaces B: Biointerfaces*, *113*, 467–476.

Kyzas, G. Z., Koltsakidou, A., Nanaki, S. G., Bikiaris, D. N., & Lambropoulou, D. A. (2015). Removal of beta-blockers from aqueous media by adsorption onto graphene oxide. *Science of the Total Environment*, *537*, 411–420.

Lai, L., Xie, Q., Chi, L., Gu, W., & Wu, D. (2016). Adsorption of phosphate from water by easily separable Fe_3O_4@ SiO_2 core/shell magnetic nanoparticles functionalized with hydrous lanthanum oxide. *Journal of Colloid and Interface Science*, *465*, 76–82.

Lian, F., Song, Z., Liu, Z., Zhu, L., & Xing, B. (2013). Mechanistic understanding of tetracycline sorption on waste tire powder and its chars as affected by Cu^{2+} and pH. *Environmental Pollution*, *178*, 264–270.

Lin, Y., Xu, S., & Li, J. (2013). Fast and highly efficient tetracyclines removal from environmental waters by graphene oxide functionalized magnetic particles. *Chemical Engineering Journal*, *225*, 679–685.

Ling, C., Liu, F.-Q., Xu, C., Chen, T.-P., & Li, A.-M. (2013). An integrative technique based on synergistic coremoval and sequential recovery of copper and tetracycline with dual-functional chelating resin: Roles of amine and carboxyl groups. *ACS Applied Materials & Interfaces*, *5*(22), 11808–11817.

Liu, Q., Zhong, L. B., Zhao, Q. B., Frear, C., & Zheng, Y. M. (2015). Synthesis of Fe_3O_4/polyacrylonitrile composite electrospun nanofiber mat for effective adsorption of tetracycline. *ACS Applied Materials & Interfaces*, *7*(27), 14573–14583.

Liu, C., Xu, J., Lee, D.-J., Yu, D., & Lihong, L. (2016). Denitrifying sulfide removal process on high-tetracycline wastewater. *Bioresource Technology*, *205*, 254–257.

Mukherjee, R., Bhunia, P., & De, S. (2016). Impact of graphene oxide on removal of heavy metals using mixed matrix membrane. *Chemical Engineering Journal*, *292*, 284–297.

Muliwa, A. M., Leswifi, T. Y., Onyango, M. S., & Maity, A. (2016). Magnetic adsorption separation (MAS) process: An alternative method of extracting Cr (VI) from aqueous solution using polypyrrole coated Fe_3O_4 nanocomposites. *Separation and Purification Technology*, *158*, 250–258.

Oladoja, N., Adelagun, R., Ahmad, A., Unuabonah, E., & Bello, H. (2014). Preparation of magnetic: Macro-reticulated cross-linked chitosan for tetracycline removal from aquatic systems. *Colloids and Surfaces B: Biointerfaces*, *117*, 51–59.

Shan, R.-r., Yan, L.-g., Yang, K., Hao, Y.-f., & Du, B. (2015). Adsorption of Cd (II) by Mg–Al–CO_3-and magnetic Fe_3O_4/Mg–Al–CO_3-layered double hydroxides: Kinetic, isothermal, thermodynamic and mechanistic studies. *Journal of Hazardous Materials*, *299*, 42–49.

Sharma, V. K., Johnson, N., Cizmas, L., McDonald, T. J., & Kim, H. (2016). A review of the influence of treatment strategies on antibiotic resistant bacteria and antibiotic resistance genes. *Chemosphere*,

Singh, S., Barick, K., & Bahadur, D. (2011). Surface engineered magnetic nanoparticles for removal of toxic metal ions and bacterial pathogens. *Journal of Hazardous Materials*, *192*(3), 1539–1547.

Tang, W.-W., Zeng, G.-M., Gong, J.-L., Liu, Y., Wang, X.-Y., Liu, Y.-Y., et al. (2012). Simultaneous adsorption of atrazine and Cu (II) from wastewater by magnetic multi-walled carbon nanotube. *Chemical Engineering Journal*, *211*, 470–478.

Tang, W.-W., Zeng, G.-M., Gong, J.-L., Liang, J., Xu, P., Zhang, C., et al. (2014). Impact of humic/fulvic acid on the removal of heavy metals from aqueous solutions using nanomaterials: A review. *Science of the Total Environment*, *468*, 1014–1027.

Travlou, N. A., Kyzas, G. Z., Lazaridis, N. K., & Deliyanni, E. A. (2013). Functionalization of graphite oxide with magnetic chitosan for the preparation of a nanocomposite dye adsorbent. *Langmuir*, *29*(5), 1657–1668.

Wang, T., Zhang, L., Li, C., Yang, W., Song, T., Tang, C., et al. (2015). Synthesis of core–shell magnetic Fe_3O_4@ poly (m-phenylenediamine) particles for chromium reduction and adsorption. *Environmental Science & Technology*, *49*(9), 5654–5662.

Wu, Z., Zhong, H., Yuan, X., Wang, H., Wang, L., Chen, X., et al. (2014). Adsorptive removal of methylene blue by rhamnolipid-functionalized graphene oxide from wastewater. *Water Research*, *67*, 330–344.

Ye, N., Xie, Y., Shi, P., Gao, T., & Ma, J. (2014). Synthesis of magnetite/graphene oxide/chitosan composite and its application for protein adsorption. *Materials Science and Engineering: C*, *45*, 8–14.

Zhang, S., Zhang, Y., Liu, J., Xu, Q., Xiao, H., Wang, X., et al. (2013). Thiol modified Fe_3O_4@SiO_2 as a robust, high effective: And recycling magnetic sorbent for mercury removal. *Chemical Engineering Journal*, *226*, 30–38.

Zhang, Z., Liu, H., Wu, L., Lan, H., & Qu, J. (2015). Preparation of amino-Fe (III) functionalized mesoporous silica for synergistic adsorption of tetracycline and copper. *Chemosphere*, *138*, 625–632.

Zhao, Y., Geng, J., Wang, X., Gu, X., & Gao, S. (2011). Adsorption of tetracycline onto goethite in the presence of metal cations and humic substances. *Journal of Colloid and Interface Science*, *361*(1), 247–251.